

# Chapter 5. CPT/ $\beta$ -CD and CPT/ $\beta$ -CD-g-Alg Inclusion complexes fabrication and characterisation

## 5.1 Synopsis

*Sodium alginate is widely used in drug delivery systems due to the unique properties they possess such as biocompatibility, bioadhesion and low toxicity. However, sodium alginate does not show any prolonged release of several drugs (as shown in [Chapter 4](#)). This chapter describes for the first time the synthesis and characterisation of camptothecin (CPT) inclusion complexes with  $\beta$ -CD (CPT/  $\beta$ -CD) and with  $\beta$ -cyclodextrin grafted sodium alginate (CPT/ $\beta$ -CD-g-Alg). The research aims to provide a more complete understanding of the CPT inclusion complexes.*

*This chapter describes the synthesis and characterisation of mono-tosyl- $\beta$ -cyclodextrin ( $\beta$ -CD-6-OTs) and tetrabutylammonium alginate (TBA-Alg) for the production of  $\beta$ -cyclodextrin grafted sodium alginate ( $\beta$ -CD-g-Alg). Here, the first reported synthesis and characterisation of (CPT) inclusion complexes with  $\beta$ -CD (CPT/  $\beta$ -CD) and with (CPT/ $\beta$ -CD-g-Alg) are described. Each are characterised using ATR-FTIR,  $^1\text{H}$  NMR and TGA spectroscopies.*

## 5.2 Synthesis and characterisation of $\beta$ -CD-6-OTs

In order to improve reactivity of the  $\beta$ -CD hydroxyl groups tosylation reaction with *p*-toluenesulfonyl chloride are often carried out. Tosylation of the  $\beta$ -CD is typically carried out to facilitate better nucleophilic substitution of the OH group [104, 116, 181].  $\beta$ -CD-6-OTs is generally prepared by the reaction of  $\beta$ -CD with *p*-toluenesulfonyl chloride in dry pyridine, or in aqueous acetonitrile, at alkaline pH [116, 181, 182]. However, this method has several disadvantages including, very poor yield of  $\beta$ -CD-6-OTs (approximately 17 %); and the  $\beta$ -CD-6-OTs must be separated from multi-tosylated  $\beta$ -CD by chromatography [183].

To overcome these disadvantages this thesis used *p*-toluenesulfonic anhydride ( $\text{Ts}_2\text{O}$ ) instead of *p*-toluenesulfonyl chloride to prepared  $\beta$ -CD-6-OTs (Figure 5.1 (Step 1(a)) [126]. The advantage of using  $\text{Ts}_2\text{O}$  to produce  $\beta$ -CD-6-OTs is that it affords pure  $\beta$ -CD-6-OTs in 61 % yield without the need for purification by chromatography [126].

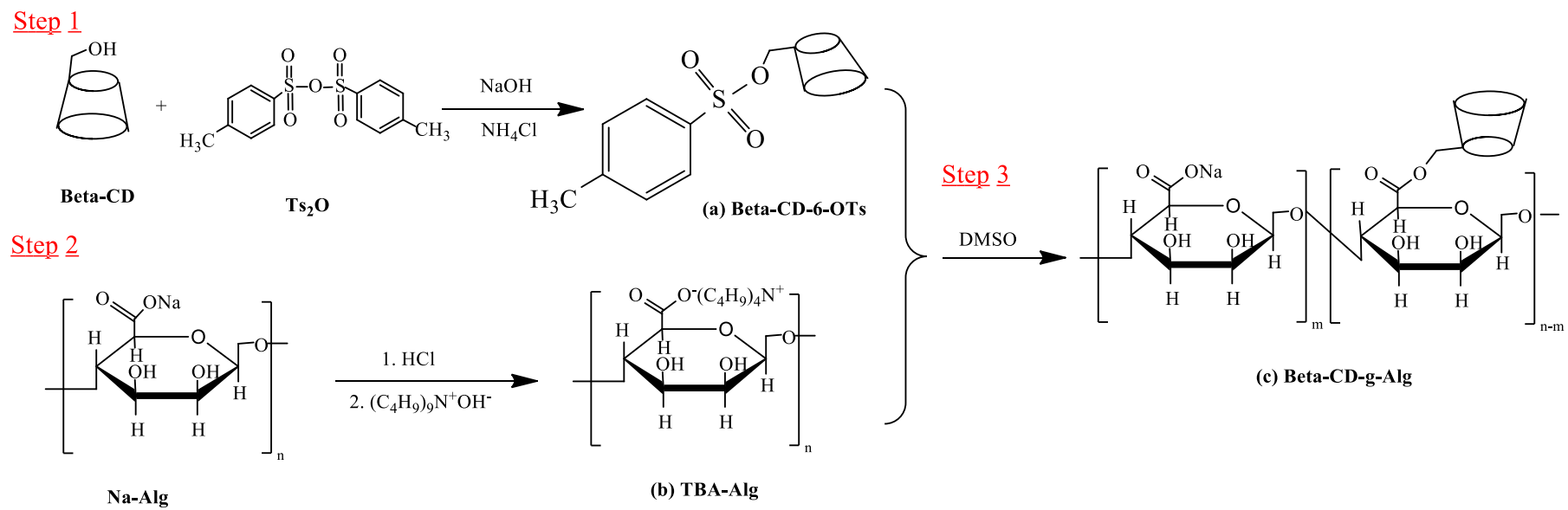


Figure 5-1 Synthesis of  $\beta$ -cyclodextrin grafted sodium alginate [128].

### 5.2.1 ATR-FTIR spectroscopic characterisation of $\beta$ -CD-6-OTs

Figure 5.2 shows the ATR-FTIR spectra of (a)  $\beta$ -CD and (b)  $\beta$ -CD-6-OTs. The spectrum of  $\beta$ -CD (Figure 5.2(a)) shows a prominent absorption peak at  $\sim 3386\text{ cm}^{-1}$  due to the -OH stretching vibration. The aliphatic -CH<sub>2</sub> stretching vibration was observed at  $2920\text{ cm}^{-1}$ . Furthermore, two peaks at  $1158\text{ cm}^{-1}$  and  $1029\text{ cm}^{-1}$  can be attributed to the presence of C-O-C and C-OH groups, respectively [184]. The spectrum of the  $\beta$ -CD-6-OTs (Figure 5.2(b)) shows characteristic absorption peaks at  $3395$ ,  $1030$  and  $1156\text{ cm}^{-1}$  for  $\beta$ -CD, which correspond to the -OH, C-OH and C-O-C groups, respectively [184]. Further, the spectrum shows a strong peak at  $1402\text{ cm}^{-1}$  due to the presence of the sulfonate group -SO<sub>2</sub>-O- (from tosylation), and a peak at  $\sim 3146\text{ cm}^{-1}$  which represents the stretching vibration of the aromatic ring of the benzyl sulphonate [185]. These results confirm that  $\beta$ -CD-6-OTs was successfully synthesised.

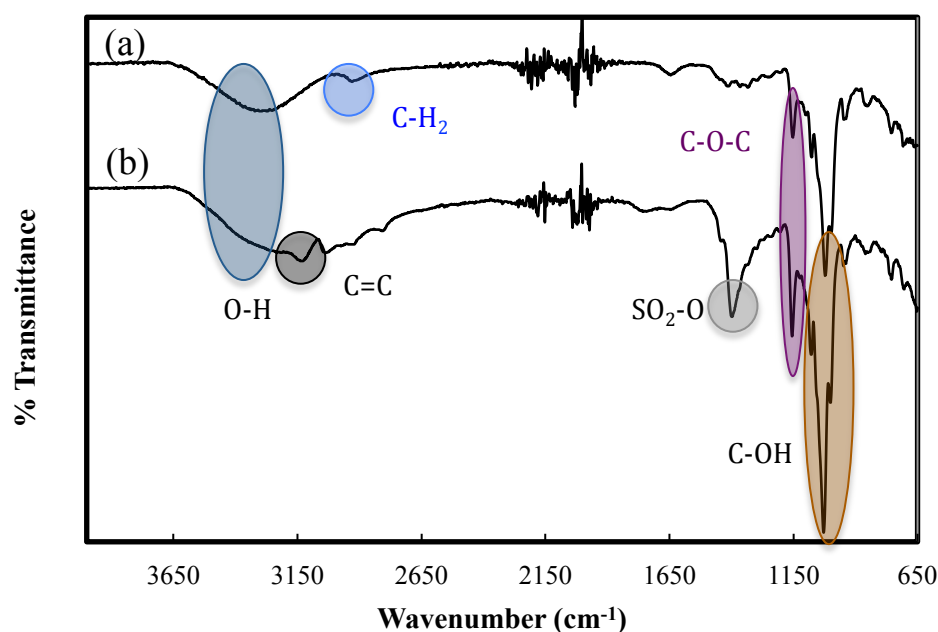


Figure 5-2 ATR-FTIR spectra of (a)  $\beta$ -CD and (b)  $\beta$ -CD-6-OTs.

### 5.3 Synthesis and characterisation of TBA-Alg

In order to increase the solubility of the Na-Alg in an organic media, it was necessary to exchange Na<sup>+</sup> cations with an organic tetrabutylammonium counterion (TBA<sup>+</sup>) The

resulting tetrabutylammonium alginate (TBA-Alg) (see [Figure 5.1 \(Step 2\(b\)\)](#)) can then be dissolved in polar aprotic solvents such as dimethylsulfoxide (DMSO) or dimethylformamide (DMF) [186]. [Figure 5.1 \(Step 2\)](#) shows that the preparation of TBA-Alg, which was synthesised as a white cotton-like compound, was achieved by the reaction between Na-Alg and TBAOH (see [Chapter 2, Section 2.11.2.1.2 for the full synthesis method](#)).

### 5.3.1 ATR-FTIR spectroscopic characterisation of TBA-Alg

[Figure 5.3](#) shows the ATR-FTIR spectra of (a) Na-Alg and (b) TBA-Alg. The spectrum of Na-Alg ([Figure 5.3\(a\)](#)) shows prominent absorption peaks at 1595 and 1403  $\text{cm}^{-1}$ , which represent the symmetric and asymmetric  $\text{COO}^-$  stretching vibration of free carboxyl groups. An O-H stretching vibration at  $\sim 3272 \text{ cm}^{-1}$  confirmed the presence of hydrogen bonding of the -OH groups. Furthermore, the peak at 1027  $\text{cm}^{-1}$  can be attributed to the presence of -C-OH stretching vibrations groups [187]. The spectrum of the TBA-Alg ([Figure 5.3\(b\)](#)) shows a broad -OH stretching vibration at  $\sim 3249 \text{ cm}^{-1}$ . The aliphatic C-H stretching vibration was observed between 2880  $\text{cm}^{-1}$  and 2960  $\text{cm}^{-1}$  and the peak at 1603  $\text{cm}^{-1}$  can be attributed to the presence of carboxylate  $\text{COO}^-$  stretching vibrations [186]. These results confirm that TBA-Alg was successfully synthesised.

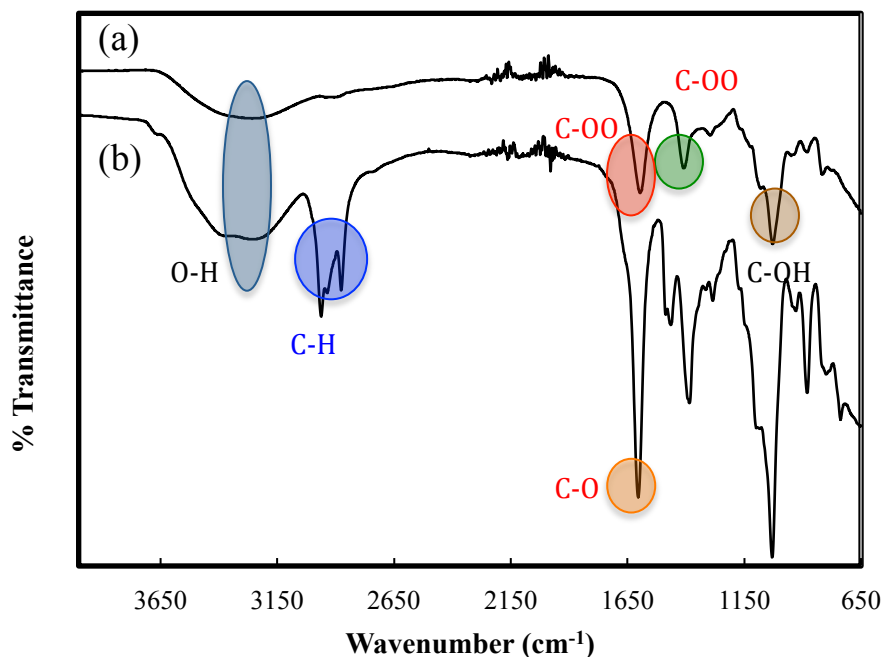


Figure 5-3 ATR-FTIR spectra of (a) Na-Alg and (b) TBA-Alg.

## 5.4 Synthesis and characterisation of $\beta$ -CD-g-Alg

Figure 5.1 (Step 3) shows the synthesis scheme of the  $\beta$ -CD-g-Alg (c) through the reaction between  $\beta$ -CD-6-OTs (a) from Figure 5.1 (Step 1) (see Section 5.2) and TBA-Alg (b) from Figure 5.1 (Step 2) (see Section 5.3) in DMSO solvent in a 1:1 molar ratio, as described previously by Zhang et al [128]. (see Chapter 2, Section 2.11.2.1.3 for the full synthesis method).

### 5.4.1 ATR-FTIR spectroscopic characterisation of $\beta$ -CD-g-Alg

Figure 5.4 shows the ATR-FTIR spectra of (a)  $\beta$ -CD-6-OTs, (b) TBA-Alg and (c)  $\beta$ -CD-g-Alg (see Chapter 2, Section 2.10.2.1.3 for the full synthesis method). The spectra of  $\beta$ -CD-6-OTs (Figure 5.4(a)) and TBA-Alg (Figure 5.4(b)) were discussed previously (Refer to Chapter 5, Section's 5.2.1 and 5.3.1 for details). The spectrum of  $\beta$ -CD-g-Alg (Fig. 5.4(c)) shows dominant peaks at  $\sim 3291$  and  $1021\text{ cm}^{-1}$  due to the presence of -OH and -C-OH stretching vibrations of the  $\beta$ -CD and Na-Alg [188]. The peak at  $1729\text{ cm}^{-1}$  represents the stretching vibration of carbonyl C=O groups. Finally, the spectrum shows the two characteristic peaks for  $\beta$ -CD at  $2929\text{ cm}^{-1}$  and  $1152\text{ cm}^{-1}$

which can be assigned to the stretching vibration of aliphatic  $-CH_2$  groups and  $-C-O-C$  stretching vibrations [184]. These results confirm that  $\beta$ -CD-g-Alg was successfully synthesised.

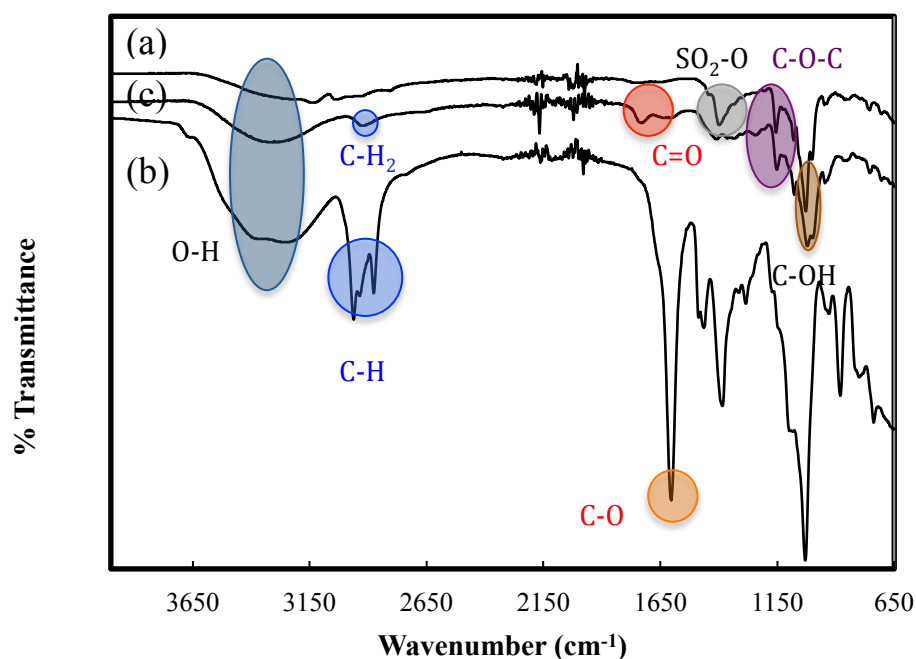


Figure 5-4 ATR-FTIR spectra of (a)  $\beta$ -CD-6-OTs, (b) TBA-Alg and (c)  $\beta$ -CD-g-Alg.

## 5.5 Synthesis and characterisation of CPT/ $\beta$ -CD and CPT/ $\beta$ -CD-g-Alg inclusion complexes

CPT was loaded into  $\beta$ -CD and  $\beta$ -CD-g-Alg to form inclusion complexes for subsequent drug delivery trials, to be discussed in [Chapter 6](#) of this thesis. The CPT/ $\beta$ -CD and CPT/ $\beta$ -CD-g-Alg inclusion complexes were prepared by a coprecipitation method, as described by Tsai et al. [105] (see [Chapter 2, Section's 2.11.1 and 2.11.2.2, respectively, for the full synthesis method](#)). The inclusion complexes were characterised by ATR-FTIR spectroscopy, <sup>1</sup>HNMR spectroscopy and TGA thermal analysis. ATR-FTIR spectroscopy is a very useful technique to prove the

formation of inclusion complexes because any change in the peak intensities of the guest (in our case the CPT) or host ( $\beta$ -CD or  $\beta$ -CD-g-Alg) can provide valuable information on the occurrence of the inclusion [189].  $^1\text{H}$  NMR spectroscopy is one of the most reliable techniques for studying the inclusion complex formation, because any change in the proton chemical shifts, or broadening of selective signals between the guest molecules and  $\beta$ -CD, gives direct evidence that the guest has entered inside the cavity of the  $\beta$ -CD [129, 190]. The following describes the results from each in detail.

## 5.5.1 Characterisation of CPT/ $\beta$ -CD inclusion complexes

### 5.5.1.1 ATR-FTIR spectroscopic characterisation of CPT/ $\beta$ -CD

Figure 5.5 shows the ATR-FTIR spectra of (a)  $\beta$ -CD, (b) CPT and (c) CPT/ $\beta$ -CD. The spectrum of  $\beta$ -CD (Figure 5.5(a)) has been discussed previously (Refer to Chapter 5, Section 5.2.1 for details). An ATR-FTIR spectrum of CPT is displayed in Figure 5.5(b). The CPT spectrum shows characteristic peaks in agreement with previously reported literature [191]. The principle peaks observed at  $1651\text{ cm}^{-1}$  and  $1737\text{ cm}^{-1}$  correspond to the stretching vibrations of the carbonyl group C=O in the ketone group and lactone ring, respectively. The aromatic C-H stretching vibration of amino quinoline was observed at  $\sim 3118\text{ cm}^{-1}$ , and the peaks appearing in the region of  $2884$ - $2975\text{ cm}^{-1}$  represent the stretching vibrations of the  $\text{CH}_3$  group. The peak at  $\sim 3426\text{ cm}^{-1}$  can be attributed to the presence of hydrogen bonding of the -OH groups. Finally, the two peaks at  $1600\text{ cm}^{-1}$  and  $1578\text{ cm}^{-1}$  are possibly from the skeletal vibrations of the phenyl rings.

Figure 5.5(c) shows the ATR-FTIR spectrum of the CPT/ $\beta$ -CD inclusion complex (see Chapter 2, Section 2.11.1 for the full synthesis method). The spectrum shows obvious changes after the complex compared to  $\beta$ -CD. The most notable is that the peak at  $\sim 3118\text{ cm}^{-1}$  corresponding to aromatic the C-H stretching vibration of amino quinoline has disappeared. The disappearance can be attributed to the steric hindrance of this group, as the molecule (CPT) is included into the  $\beta$ -CD cavity [104]. Interestingly, the remaining C=O peaks from the ketone group and lactone ring vibrations at  $1651\text{ cm}^{-1}$  and  $1738\text{ cm}^{-1}$  still remained in the spectrum after complex formation. This implies that the part of the CPT molecule with the amino quinoline is

included into the  $\beta$ -CD cavity while the lactone part of the molecule is sticking out. Finally, the two peaks at  $\sim 3296\text{ cm}^{-1}$  and  $1152\text{ cm}^{-1}$  represent the stretching vibration of -OH group and C-O-C stretching vibrations, respectively, of  $\beta$ -CD. These results confirmed that CPT was successfully included inside the  $\beta$ -CD to form a CPT/ $\beta$ -CD inclusion complex [184, 189].

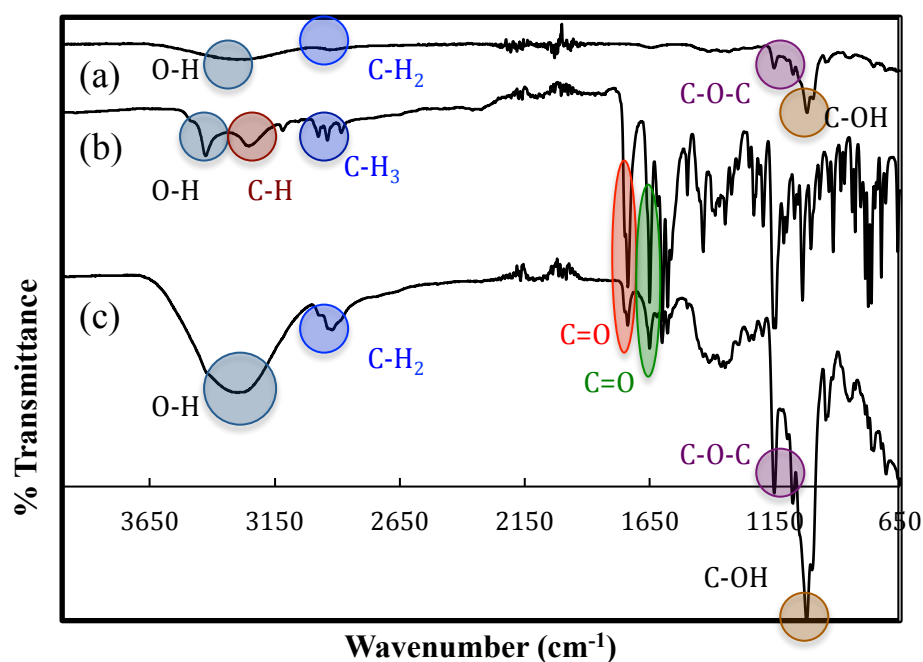


Figure 5-5 ATR-FTIR spectra of (a)  $\beta$ -CD, (b) CPT and (c) a CPT/ $\beta$ -CD inclusion complex.

### 5.5.1.2 $^1\text{H}$ NMR spectroscopic characterisation of CPT/ $\beta$ -CD inclusion complexes

$^1\text{H}$  NMR characterisation was performed in deuterium oxide ( $\text{D}_2\text{O}$ ) as the  $^1\text{H}$  NMR solvent. Figure 5.6 shows the  $^1\text{H}$  NMR spectra of both the (a)  $\beta$ -CD and (b) CPT/ $\beta$ -CD inclusion complexes. In this study only the chemical shifts of  $\beta$ -CD protons in the absence and in the presence of CPT molecules were investigated. The chemical shifts are shown in Table 5.1. As can be seen from Figure 5.6 the inclusion complexation of  $\beta$ -CD with CPT exhibited significant changes in the chemical shift ( $0.0268 - 0.0125$  ppm) of the H-3 and H-5 protons, which are located in the interior of the  $\beta$ -CD cavity (see Chapter 1, Figure 1.15). In contrast, there were negligible shifts in the H-1, H-2, H-4 and H-6 protons, located in the exterior of the  $\beta$ -CD cavity, [190]. The signals for

the H-3 and H-5 protons displayed downfield shifts in the presence of CPT molecules compared to pure  $\beta$ -CD [192]. Moreover, the chemical shifts of the H-3 protons (0.0268 ppm) were slightly higher than the H-5 proton chemical shifts (0.0125 ppm) [190].

The detailed  $^1\text{H}$  NMR spectroscopy study of  $\beta$ -CD in the presence, and absence, of CPT molecules confirmed the inclusion of CPT into the  $\beta$ -CD cavity due to the observed shifts in the  $\beta$ -CD cavity protons compared to the other external protons of  $\beta$ -CD [129, 190, 192]. Also, the higher chemical shifts in the  $\beta$ -CD cavity protons implies that the CPT/ $\beta$ -CD inclusion complex is stable [192].

Furthermore, the change in the chemical shift of the H-3 (0.0268 ppm), which is closer to the wider rim is slightly higher than the change in the H-5 proton chemical shift (0.0125 ppm), which is closer to the narrowest part of the  $\beta$ -CD (see [Chapter 1, Figure 1.15](#)). This result indicates that the amino quinoline group for the CPT molecule is included into the  $\beta$ -CD cavity from the wider rim as shown in [Figure 5.7](#) [189]. The same result was also concluded from the ATR-FTIR result as shown previously.

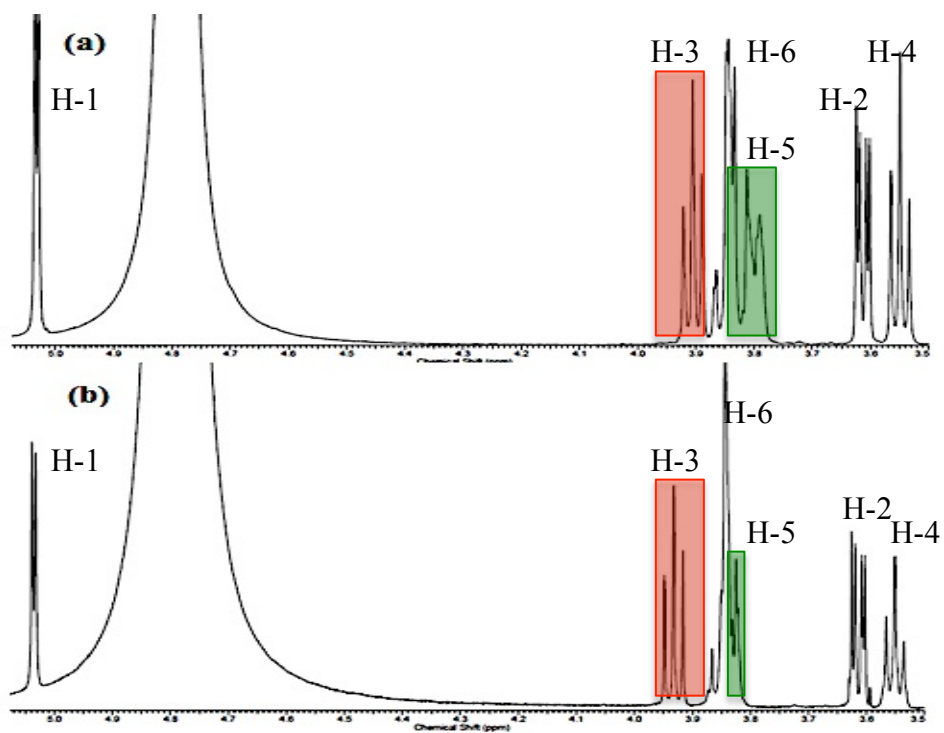


Figure 5-6  $^1\text{H}$  NMR spectroscopy spectra of (a)  $\beta$ -CD and (b) a CPT/ $\beta$ -CD inclusion complexes.

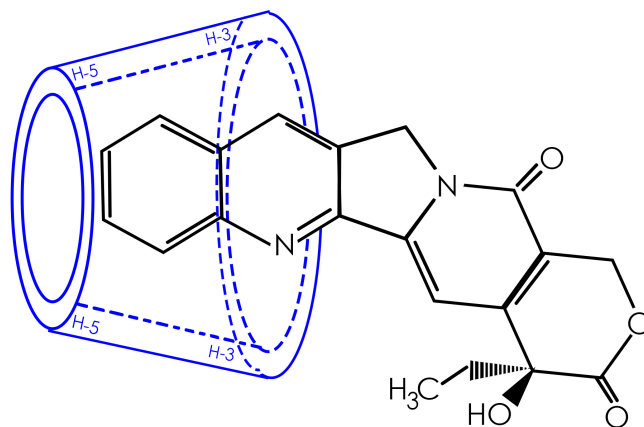


Figure 5-7 Simplified model of CPT/ $\beta$ -CD inclusion complex, (Note: OH groups not represented on the  $\beta$ -CD).

Table 5-<sup>1</sup>H NMR chemical shifts ( $\delta$  /ppm) for the protons of  $\beta$ -CD (free) and CPT/ $\beta$ -CD (complex) inclusion complex.

$\beta$ -CD	$\delta_{\text{free}}$ (ppm)	$\delta_{\text{complex}}$ (ppm)	$\Delta \delta$ (ppm)
H-1	5.0323	5.0352	0.0029
H-2	3.6242	3.6255	0.0013
H-3	3.9056	3.9324	<u>0.0268</u>
H-4	3.5492	3.5511	0.0019
H-5	3.8124	3.8249	<u>0.0125</u>
H-6	3.8444	3.8439	-0.0005

### 5.5.1.3 Thermogravimetric analysis (TGA) of CPT/ $\beta$ -CD inclusion complexes

For thermal analysis a CPT/ $\beta$ -CD inclusion complex was prepared as described in [Chapter 2, Section 2.13.3.1](#). TGA thermograms of the (a) CPT, (b)  $\beta$ -CD and (c) CPT/ $\beta$ -CD are displayed in [Figure 5.8](#). The initial decomposition temperature ( $T_i$ ) and the final decomposition temperature ( $T_f$ ) as well as the weight loss for each stage of the decomposition can be found in [Table 5.2](#). More importantly is the mass loss of the compounds marked as first stage, second stage and third stage on [Figure 5.8](#). These stages will be explained in detail in the following. As can be seen from [Figure 5.8](#) the basic shapes of curves b and c remain similar, but there is a considerable difference between them in the weight losses including water release, decomposition and residual weight.

In the first stage, the  $T_i$  and  $T_f$  decomposition for  $\beta$ -CD ([Figure 5.8\(b\)](#)) and CPT/ $\beta$ -CD ([Figure 5.8\(c\)](#)) was 40 °C and 115 °C, with a weight loss of 14 % wt/wt and 40 °C and 90 °C, with a weight loss of 8 % wt/wt, respectively. The weight loss observed in

this stage can be related to the water loss (included or physisorbed water) [193-195]. As can be seen from [Figure 5.8\(a\)](#) the  $T_i$  and  $T_f$  of the CPT In the second stage, were 260 °C and 270 °C, respectively, with a weight loss of 15 % wt/wt.

In the third stage, the  $T_i$  and  $T_f$  decomposition of CPT was 270 °C and 390 °C, respectively, with weight loss 77 % wt/wt. The observed weight loss may indicate to the thermal decarboxylation of CPT molecules [196]. It is clear that the CPT exhibits the highest stability compared to  $\beta$ -CD ([Figure 5.8\(b\)](#)) and CPT/ $\beta$ -CD ([Figure 5.8\(c\)](#)). This reflects that the thermal stability of the CPT inclusion complex is lower than of CPT, which is in accordance with the observation in literature [195]. Furthermore, CPT decomposes showed the lower residual weight (8 %).

The  $T_i$  and  $T_f$  decomposition for  $\beta$ -CD and CPT/ $\beta$ -CD in the third stage was 290 °C and 565 °C, with a weight loss of 72 % wt/wt and 265 °C and 565 °C, with a weight loss of 81 % wt/wt, respectively. The weight loss observed in this stage can be explained by the decomposition of the  $\beta$ -CD and CPT/ $\beta$ -CD structure [193, 194]. It is observed that the  $T_i$  of the decomposition stage is shifted from 290 °C in  $\beta$ -CD to 265 °C in  $\beta$ -CD after formation of the inclusion complex may due to the presence of CPT. Finally, the residual weight of  $\beta$ -CD and CPT/ $\beta$ -CD was 14 % wt/wt and 11 % wt/wt, respectively.

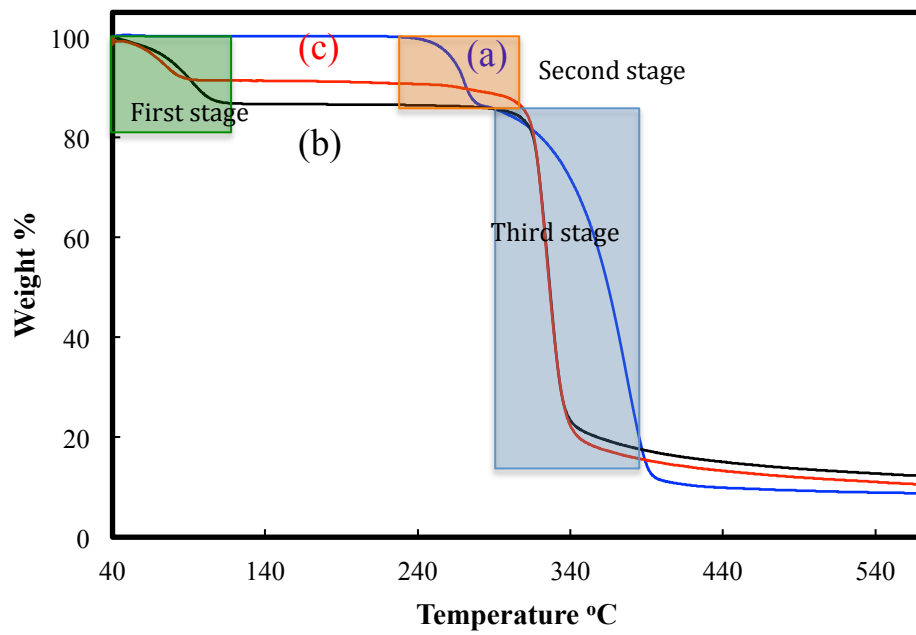


Figure 5-8 TGA thermograms of (a) CPT, (b)  $\beta$ -CD and (c) CPT/ $\beta$ -CD.

Table 5-2 The  $T_i$  and  $T_f$  decomposition temperatures ( $^{\circ}\text{C}$ ) as well as the weight loss accompanying the stage of decomposition for CPT,  $\beta$ -CD and CPT/  $\beta$ -CD.

Compounds	Stage	TGA		Weight loss (% wt/wt)	Residual weight (% wt/wt)
		$T_i$ $^{\circ}\text{C}$	$T_f$ $^{\circ}\text{C}$		
CPT	1 <sup>st</sup>	-	-	-	8
	2 <sup>nd</sup>	260	270	15	
	3 <sup>rd</sup>	270	390	77	
$\beta$ -CD	1 <sup>st</sup>	40	115	14	14
	2 <sup>nd</sup>	-	-	-	
	3 <sup>rd</sup>	290	565	72	
CPT/ $\beta$ -CD	1 <sup>st</sup>	40	90	8	11
	2 <sup>nd</sup>	-	-	-	
	3 <sup>rd</sup>	265	565	81	

## 5.5.2 Characterisation of CPT/ $\beta$ -CD-g-Alg complexes

### 5.5.2.1 ATR-FTIR spectroscopic characterisation of CPT/ $\beta$ -CD-g-Alg

Figure 5.9 shows the ATR-FTIR spectra of (a)  $\beta$ -CD-g-Alg, (b) CPT and (c) CPT/  $\beta$ -CD-g-Alg. The spectra of  $\beta$ -CD-g-Alg (Figure 5.9(a)) and CPT (Figure 5.9(b)) have been discussed previously (Refer to Chapter 5, Section's 5.4.1 and 5.5.1.1, respectively, for details). An ATR-FTIR spectrum of CPT/  $\beta$ -CD-g-Alg is displayed in Figure 5.9(c). The spectrum shows obvious changes after the complex was formed.

The peaks of the ketone group and lactone ring vibrations at  $1650\text{ cm}^{-1}$  and  $1737\text{ cm}^{-1}$  still appear in the spectrum after the complex was formed, whereas the aromatic C-H stretching vibration of amino quinoline disappeared. Hence it may be inferred that CPT is included into the cavity of  $\beta$ -CD in the  $\beta$ -CD-g-Alg. Finally, the two peaks at  $\sim 3426\text{ cm}^{-1}$  and  $1150\text{ cm}^{-1}$  represent the stretching vibration of the -OH group and C-O-C stretching vibrations, respectively, of  $\beta$ -CD. These results indicate that the inclusion complex between  $\beta$ -CD in the  $\beta$ -CD-g-Alg and CPT has most likely formed [116].

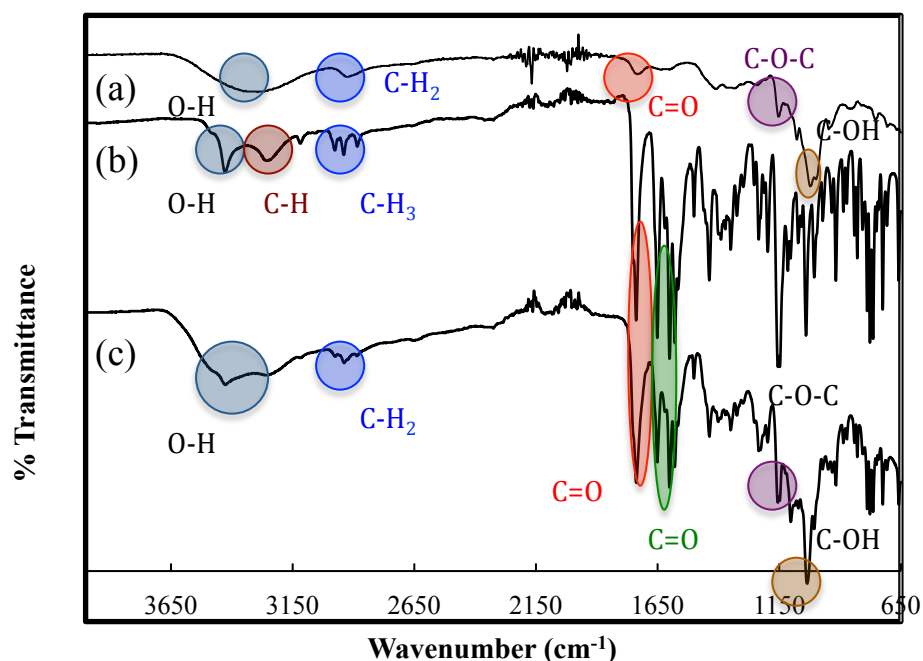


Figure 5-9 ATR-FTIR spectra of (a)  $\beta$ -CD-g-Alg, (b) CPT and (c) CPT/  $\beta$ -CD-g-Alg inclusion complex.

### 5.5.2.2 $^1\text{H}$ NMR spectroscopic characterisation of CPT/ $\beta$ -CD-g-Alg inclusion complexes

#### 5.5.2.2.1 $^1\text{H}$ NMR spectroscopic characterisation of $\beta$ -CD-g-Alg

$\beta$ -CD-g-Alg was prepared by the reaction between  $\beta$ -CD-6-OTs and TBA-Alg (see Chapter 2, Section 2.11.2.1.3 for the full synthesis method).  $^1\text{H}$  NMR characterisation was performed in deuterated dimethylsulphoxide ( $d_6$ -DMSO) as the  $^1\text{H}$  NMR solvent. Figure 5.10 shows the  $^1\text{H}$  NMR spectrum of  $\beta$ -CD-g-Alg. The spectrum of  $\beta$ -CD-g-Alg showed the characteristics signals of both Na-Alg and  $\beta$ -CD. As can be seen from

Figure 5.10 the spectrum showed a chemical shift located down-field at 5.73 ppm and 5.68 ppm can be assigned to the H-1 protons of guluronic acid (H-1G) and H-1 protons of mannuronic acid (H-1M), respectively [197, 198]. The signal at 4.84 ppm can be attributed to H-5 proton of guluronic acid (H-5G) and to the H-1 proton of  $\beta$ -CD [199]. The signal at 4.45 ppm can be assigned to H-2 and H-3 protons of mannuronic (H-2M) and guluronic acid (H-3G), respectively [198]. The signals located between 3.55-3.70 ppm can be assigned to H-2, H-3, H-4, H5 and H-6 of  $\beta$ -CD [189, 199].

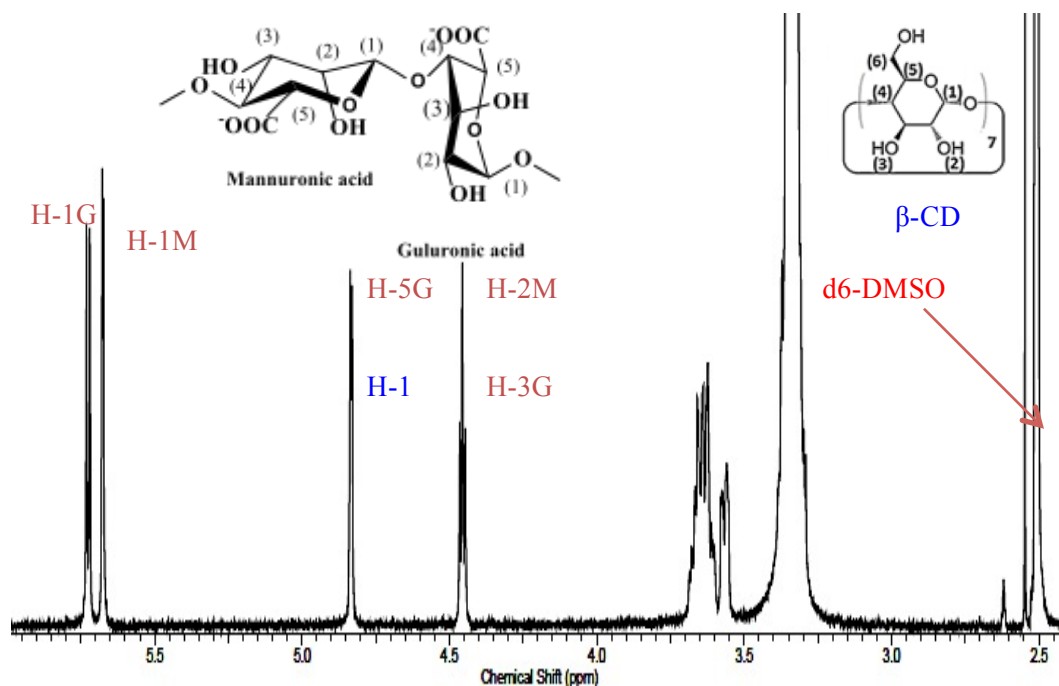


Figure 5-10  $^1\text{H}$  NMR spectra of  $\beta\text{-CD-g-Alg}$ .

#### 5.5.2.2.2 $^1\text{H}$ NMR spectroscopic characterisation of CPT/ $\beta\text{-CD-g-Alg}$ inclusion complexes

$^1\text{H}$  NMR characterisation of the CPT/ $\beta\text{-CD-g-Alg}$  inclusion complex was performed in  $\text{d}_6\text{-DMSO}$  due to the lower solubility of CPT in  $\text{D}_2\text{O}$ . In this study only the chemical shifts of the CPT protons in the absence and in the presence of  $\beta\text{-CD-g-Alg}$  were investigated due to the proton signals of  $\beta\text{-CD-g-Alg}$  (3.55 -5.8 ppm) being too faint to be observed, as can be seen from [Figure 5.11](#).

[Figure 5.11](#) shows the  $^1\text{H}$  NMR spectra of the CPT/ $\beta\text{-CD-g-Alg}$  inclusion complex. The chemical shifts are shown in [Table 5.3](#). The signals located at 0.8869 and 1.8831 ppm ([Figure 5.11](#)) can be assigned to H-18 and H-19 of the CPT molecule, respectively [200]. While the signals between 5.3083 ppm and 8.7053 ppm can be assigned to the rest of CPT protons (H-5, H-7, H-9, H-10, H-11, H-12, H-14, H-17 and O-H) [200]. Encouragingly, as can be seen from [Table 5.3](#), all the CPT protons display chemical shift changes upon complexation with  $\beta\text{-CD-g-Alg}$ . As shown in [Table 5.3](#), the change in chemical shift of the phenyl protons H-10, H-11 and H-12

was 0.0075, 0.0080 and 0.0069 ppm, respectively. It is clear to see that the change in chemical shift of the phenyl protons is slightly higher than the change in the E-ring protons H-17 chemical shift (0.0022 ppm) and the aliphatic protons H-18 and H-19 chemical shift (0.0007 and 0.0020 ppm, respectively). This result implies that the CPT/ $\beta$ -CD-g-Alg inclusion complex has formed.

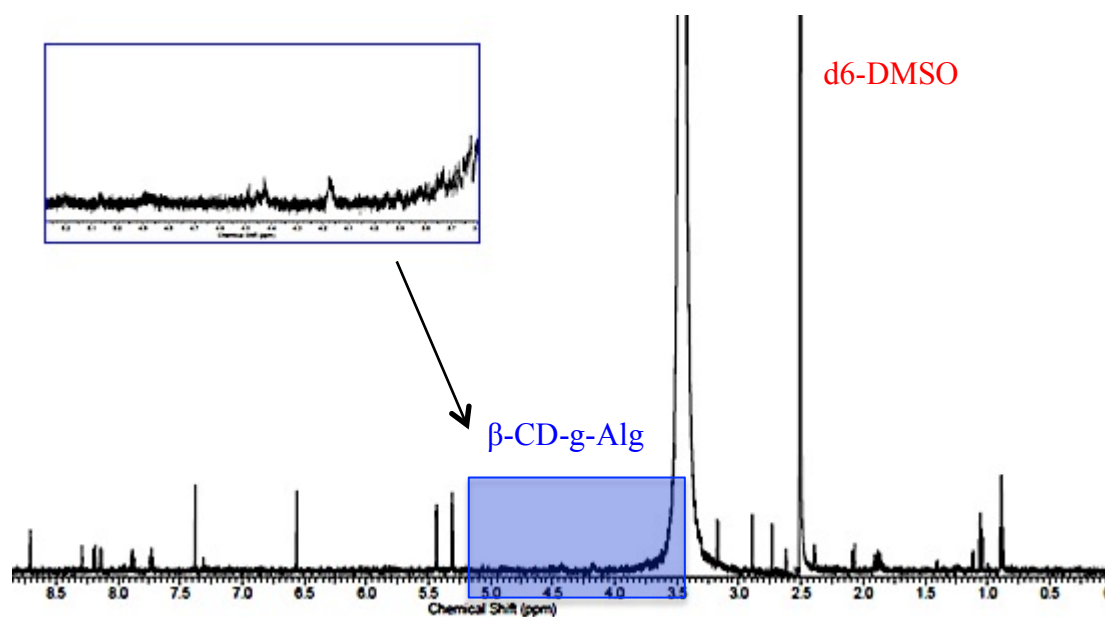


Figure 5-11  $^1\text{H}$  NMR spectra of a CPT/ $\beta$ -CD-g-Alg inclusion complex.

Table 5-3 <sup>1</sup>H NMR chemical shifts ( $\delta$  /ppm) for the protons of CPT (free) and CPT/ $\beta$ -CD-g-Alg inclusion complex (complex).

<b>CPT</b>	<b><math>\delta_{\text{free}}</math> (ppm)</b>	<b><math>\delta_{\text{complex}}</math> (ppm)</b>	<b><math>\Delta \delta</math> (ppm)</b>
<b>H-5</b>	5.3022	5.3083	0.0061
<b>H-7</b>	8.7022	8.7053	0.0031
<b>H-9</b>	8.1447	8.1439	-0.0008
<b>H-10</b>	7.7217	7.7292	<u>0.0075</u>
<b>H-11</b>	7.8749	7.8829	<u>0.0080</u>
<b>H-12</b>	8.1881	8.1950	<u>0.0069</u>
<b>H-14</b>	7.3592	7.3769	0.0177
<b>H-17</b>	5.4332	5.4354	0.0022
<b>H-18</b>	0.8862	0.8869	0.0007
<b>H-19</b>	1.8811	1.8831	0.0020
<b>O-H</b>	6.5239	6.5606	0.0367

### 5.5.2.3 TGA analysis of a CPT/ $\beta$ -CD-g-Alg inclusion complex

A CPT/ $\beta$ -CD-g-Alg inclusion complex was prepared for thermal analysis, as described in Chapter 2, section 2.13.3. TGA thermograms of the (a) CPT, (b)  $\beta$ -CD, (c) Na-Alg and (d) CPT/  $\beta$ -CD-g-Alg are displayed in Figure 5.12. The thermograms of CPT (Figure 5.12(a)) and  $\beta$ -CD (Figure 5.12(b)) were discussed previously (Refer to Chapter 5, Section 5.5.1.3 for details). The thermograms of Na-Alg (Figure 5.12(c)) and CPT/  $\beta$ -CD-g-Alg (Figure 5.12(d)) show three decomposition stages. The  $T_i$  and  $T_f$  decomposition as well as the weight loss for each stage of the decomposition can be found in Table 5.4. In the first stage, which is related to the dehydration of Na-Alg and CPT/  $\beta$ -CD-g-Alg, the temperature of  $T_i$  and  $T_f$  decomposition was 40 °C and 202 °C, with a weight loss of 13 % wt/wt and 40 °C and 53 °C, with a weight loss of 10 % wt/wt, respectively [187].

In the second stage, the  $T_i$  and  $T_f$  decomposition for Na-Alg and CPT/  $\beta$ -CD-g-Alg was 202 °C and 290 °C, with a weight loss of 36 % wt/wt and 148 °C and 328 °C, with a weight loss of 60 % wt/wt, respectively. The weight loss can be attributed to the decomposition of the Na-Alg and CPT/  $\beta$ -CD-g-Alg structure [187]. As shown in Figure 5.12 the  $T_f$  temperature of the decomposition stage is shifted from 209 °C in Na-Alg to 328 °C in CPT/  $\beta$ -CD-g-Alg and CPT/  $\beta$ -CD-g-Alg showed a much higher weight loss (60 % wt/wt) rather than Na-Alg (36 % wt/t). This result suggested that the CPT/ $\beta$ -CD-g-Alg exhibits high thermal stability compared to Na-Alg. This observation indicates that  $\beta$ -CD increased the stability of Na-Alg [195]. Moreover, the percent of Na-Alg in CPT/  $\beta$ -CD-g-Alg appears to be approximately 40 % wt/wt. As can be seen from Figure 5.12 when the samples decompose rapidly, the curve b is always presented at the left side of the curves c and d, implying that  $\beta$ -CD (Figure 5.12(b)) exhibits the highest thermal stability compared to Na-Alg (Figure 5.12(c)) and CPT/  $\beta$ -CD-g-Alg (Figure 5.12(d)) [195]. Furthermore, the percent of  $\beta$ -CD in CPT/  $\beta$ -CD-g-Alg appears to be approximately 20 % wt/wt, so the ratio of Na-Alg to  $\beta$ -CD appears to be 2:1.

In the third stage, the  $T_i$  and  $T_f$  decomposition for Na-Alg and CPT/  $\beta$ -CD-g-Alg was 290 °C and 565 °C, with a weight loss of 13 % wt/wt and 328 °C and 565 °C, with a weight loss of 6 % wt/wt, respectively. The weight loss in this stage can be explained

by the decomposition of Na-Alg to  $\text{Na}_2\text{CO}_3$  [187]. It can be clearly seen that the CPT/ $\beta$ -CD-g-Alg inclusion complex showed lower residuals (6 % wt/wt). This is due to the decrease of  $\text{Na}^+$  ion content in the CPT/ $\beta$ -CD-g-Alg as  $\beta$ -CD has taken up some of the positions along the alginate chain as discussed previously the ratio is a 2:1 Na-Alg to  $\beta$ -CD. Finally, the residual weight of Na-Alg and CPT/ $\beta$ -CD-g-Alg was 38 % wt/wt and 24 % wt/wt, respectively, which reflects the lower  $\text{Na}^+$  ion content.

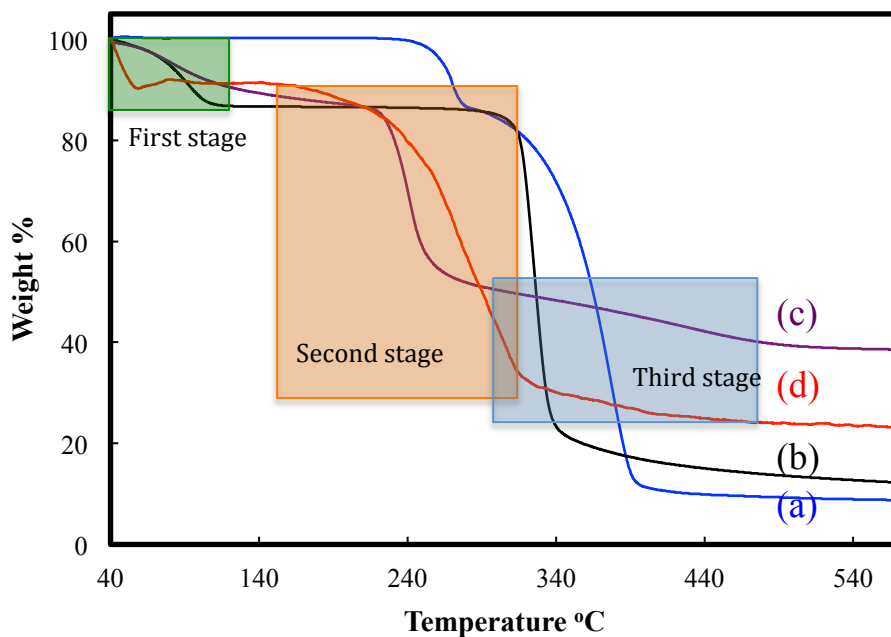


Figure 5-12 TGA thermograms of (a) CPT, (b)  $\beta$ -CD and (c) Na-Alg and (d) CPT/ $\beta$ -CD-g-Alg inclusion complex.

Table 5-4 The  $T_i$  and  $T_f$  decomposition temperatures ( $^{\circ}\text{C}$ ) as well as the weight loss accompanying each stage of decomposition for Na-Alg and CPT/  $\beta$ -CD-g-Alg inclusion complex.

Compounds	Stage	TGA		Weight loss (% wt/wt)	Residual weight (% wt/wt)
		$T_i$ $^{\circ}\text{C}$	$T_f$ $^{\circ}\text{C}$		
Na-Alg	1 <sup>st</sup>	40	202	13	38
	2 <sup>nd</sup>	202	290	36	
	3 <sup>rd</sup>	290	565	13	
CPT/ $\beta$ -CD-g-Alg	1 <sup>st</sup>	40	53	10	24
	2 <sup>nd</sup>	148	328	60	
	3 <sup>rd</sup>	328	565	6	

## 5.6 Concluding remarks

This chapter investigated the synthesis of a new drug carrier made of  $\beta$ -CD-g-Alg for a poorly water-soluble drug (CPT).  $\beta$ -CD-6-OTs was first produced to facilitate the nucleophilic substitution of the OH group on the C6 carbon of  $\beta$ -CD. ATR-FTIR spectroscopy confirmed the preparation of  $\beta$ -CD-6-OTs. Due to the poor solubility of Na-Alg, TBA-Alg was synthesised by exchanging  $\text{Na}^+$  cations in the alginate structure with an organic tetrabutylammonium counterion ( $\text{TBA}^+$ ) in order to increase the solubility of Na-Alg in an organic media. Synthesis of the TBA-Alg was characterised and confirmed by ATR-FTIR spectroscopy.  $\beta$ -CD-g-Alg was then synthesised by the reaction between  $\beta$ -CD-6-OTs and TBA-Alg. ATR-FTIR spectroscopy confirmed the synthesis of  $\beta$ -CD-g-Alg.

CPT inclusion complexes were then fabricated with  $\beta$ -CD and  $\beta$ -CD-g-Alg. The ATR-FTIR and  $^1\text{H}$  NMR spectroscopies confirmed that the two inclusion complexes were produced. ATR-FTIR spectroscopy showed that the disappearance of the amino quinoline peak confirmed the preparation of the inclusion complexes.  $^1\text{H}$  NMR spectroscopy showed that the inclusion complexation of  $\beta$ -CD with CPT exhibited a significant change in the chemical shifts for H-3 and H-5, which are located in the interior of the  $\beta$ -CD. This observation confirmed that the CPT/ $\beta$ -CD inclusion complex was produced. The results indicated that the amino quinoline group for CPT molecule is included into the  $\beta$ -CD cavity away from the wider rim. Furthermore, CPT/ $\beta$ -CD and CPT/ $\beta$ -CD-g-Alg inclusion complexes were characterised by thermogravimetric TGA analysis. It is found that  $\beta$ -CD exhibits the highest thermal stability compared to Na-Alg and CPT/ $\beta$ -CD-g-Alg. Also, it is found the thermal stability of Na-Alg increased in the presence of  $\beta$ -CD. Furthermore, the thermal analysis shows that the ratio of Na-Alg to  $\beta$ -CD appears to be 2:1.

In the next chapter ([Chapter 6](#)) studies of the release of CPT from the CPT/  $\beta$ -CD and CPT/ $\beta$ -CD-g-Alg inclusion complexes are discussed.